


A Novel PET Probe for Brown Adipose Tissue Imaging in Rodents

Hui Wang,¹ Mengzhe Wang,¹ Kantapat Chansaenpak,¹ Yang Liu,² Hong Yuan,^{1,3} Jin Xie,⁴ Hang Yin,² Rosa T. Branca,^{3,5} Zibo Li,^{1,3} Zhanhong Wu^{1,3} 

¹Department of Radiology and Biomedical Research Imaging Center, University of North Carolina at Chapel Hill, Chapel Hill, NC, 27599, USA

²Center for Molecular Medicine, Department of Biochemistry and Molecular Biology, The University of Georgia, Athens, GA, 30602, USA

³Biomedical Research Imaging Center, University of North Carolina at Chapel Hill, Chapel Hill, NC, 27599, USA

⁴Department of Chemistry, Bio-Imaging Research Center, The University of Georgia, Athens, GA, 30602, USA

⁵Department of Physics and Astronomy, University of North Carolina at Chapel Hill, Chapel Hill, NC, 27599, USA

Abstract

Purpose: Brown adipose tissue (BAT) has emerged as a promising target to counteract obesity and its associated metabolic disorders. However, the detection of this tissue remains one of the major roadblocks.

Procedures: In this study, we assess the use of BODIPY 1 as a positron emission tomography (PET) imaging agent to image BAT depots *in vivo* in two mouse phenotypes: obesity-resistant BALB/c mice and the obesity-prone C57BL/6 mice. [¹⁸F]BODIPY 1 is a radioactive dye that processed both radioactivity for PET imaging and fluorescence signal for *in vitro* mechanism study.

Results: Through the co-staining of cancer cells with BODIPY 1 and MitoTracker, we found BODIPY 1 mainly accumulated in cell mitochondria *in vitro*. Fluorescence imaging of primary brown and white adipocytes further confirmed BODIPY 1 had significantly higher accumulation in primary brown adipocytes compared with primary white adipocytes. We evaluated [¹⁸F]BODIPY 1 for BAT imaging in both obesity-resistant BALB/c mice and obesity-prone C57BL/6 mice. Indeed, [¹⁸F]BODIPY 1 was efficiently taken up by BAT in both mouse genotypes (6.40 ± 1.98 %ID/g in obesity-resistant BALB/c mice ($n=8$) and 5.37 ± 0.82 %ID/g in obesity-prone C57BL/6 mice ($n=7$)). Although norepinephrine stimulation could increase the absolute BAT uptake, the enhancement is not significant in both genotypes ($p > 0.05$) at current sample size. These results suggest BAT uptake of [¹⁸F]BODIPY 1 may be independent of BAT thermogenic activity. As a comparison, 2-deoxy-2-[¹⁸F]fluoro-D-glucose ([¹⁸F]FDG) PET imaging was performed in obesity-resistant BALB/c mice. Significantly increased uptake was observed in adrenergically activated BAT (10.08 ± 2.52 %ID/g, $n=3$) but not in inactive BAT (3.803 ± 0.70 %ID/g; $n=3$). Because [¹⁸F]BODIPY 1 maintained its fluorescent property, BAT tissue was excised and studied using fluorescence microscopy. Strong fluorescence signal was observed in BAT mouse that was injected with BODIPY 1.

Conclusions: Unlike [¹⁸F]FDG, [¹⁸F]BODIPY 1 showed prominent accumulation in BAT under both inactive and stimulated status. [¹⁸F]BODIPY 1 may serve as a valuable BAT PET agent to possibly assess BAT mitochondria density, thus BAT thermogenic capacity after further evaluation.

Key words: Brown adipose tissue, BODIPY, Positron emission tomography, Thermogenesis

Hui Wang and Mengzhe Wang contributed equally to this work.

Correspondence to: Zhanhong Wu; e-mail: zhanhong_wu@med.unc.edu

Introduction

Ectopic fat accumulation plays a critical role in the development of an unfavorable metabolic and cardiovascular disease. Adipose tissue includes two distinct types: white adipose tissue (WAT) and brown adipose tissue (BAT). It is well recognized that BAT is present and active in human newborns and is responsible for maintaining body temperature without shivering [1]. Recently, it has been shown that BAT is also present and active in a significant fraction of adult humans. The ability of this tissue to regulate body weight and glucose homeostasis makes BAT an attractive target for obesity and diabetes treatments [2, 3]. In rodents, for example, BAT is known to clear lipids from plasma and to protect from hyperlipidemia [4]. BAT also improves whole-body glucose homeostasis, as ablation of insulin receptors in BAT results in a diabetic phenotype with fasting hyperglycemia and impaired glucose tolerance [5].

BAT is an important regulator of glucose and insulin homeostasis and activated BAT exhibits increased energy expenditure. Therefore, BAT has emerged as an attractive target for the treatment of obesity [3, 6–9], especially for obese patients who failed to respond to conventional treatment methods (healthy eating and intensified exercise) or pharmaceutical interventions. In addition, BAT serves as a new target for metabolic diseases, such as type II diabetes [10–13].

Because of the increasing recognition of BAT role in several physiological and pathological processes, non-invasive imaging techniques, including positron emission tomography (PET), single-photon emission computerized tomography (SPECT), x-ray computed tomography (CT), magnetic resonance imaging (MRI), and multimodal imaging, which can potentially assess BAT-targeting drug effects, visualize BAT activity, and estimate the quantity of “burned” calories by BAT are highly desirable. Non-invasive BAT imaging can be a useful technique to quickly determine the efficacy of BAT-targeting drugs.

Brown adipocytes are characterized by an abundance of mitochondria, high expression of the uncoupling protein-1 (UCP-1), and high glucose uptake after activation [14]. PET imaging is a non-invasive, sensitive, and quantitative technique for probing a variety of biological processes and it is not surprising that, to investigate the physiology and pathology of BAT, several PET probes have been developed and tested. Despite 2-deoxy-2- ^{18}F fluoro-D-glucose (^{18}F FDG) being the probe most commonly used to detect the presence of active BAT and its glucose uptake, the metabolic role of glucose in BAT is not well understood [15, 16]. Therefore, other PET probes have been devised and tested. For example, ^{15}O H₂O has been used to evaluate the local blood flow/perfusion, as well as oxygen utilization in BAT [17]; meta- ^{123}I iodobenzylguanidine (MIBG), ^3H tetraphenylphosphonium (^3H TPP) compound [18], and 6- ^{18}F fluorodopamine (^{18}F FDA), which were originally developed as tracers for neuroendocrine tumors, are used to visualize BAT [19, 20]. SPECT/CT with

$^{99\text{m}}\text{Tc}$ sestamibi or $^{99\text{m}}\text{Tc}$ tetrofosmin has been used to visualize BAT because of their mitochondria-targeting properties [21, 22]. In the present study, we evaluated the potency of ^{18}F BODIPY 1 to visualize BAT using PET imaging. Thanks to the unique radioactive/fluorescence property of the BODIPY agent, validation of *in vivo* PET imaging results by *ex vivo* fluorescent microscopy was also performed.

Materials and Methods

General

All chemicals obtained commercially were of analytical grade and used without further purification. Analytical reversed-phase high-performance liquid chromatography (RP-HPLC) using a Gemini 5 μ C18 column (250 \times 4.6 mm) was performed on a SPD-M30A photodiode array detector (Shimadzu) and model 105S single-channel radiation detector (Carroll & Ramsey Associates).

Preparation of ^{18}F BODIPY 1

The ^{18}F -labeled BODIPY 1 was synthesized according to our previously reported procedure [23]. Briefly, 800 μg (2.1 μmol) of BODIPY 1 precursor was dissolved in 40 μl MeCN. Two microliters of SnCl₄ was added and pipetted to form a clear solution. Then 24.05 GBq of tetra-n-butylammonium ^{18}F fluoride was added to the solution and the mixture was sealed and heated to 85 $^\circ\text{C}$ for 10 min. Then the reaction was purified by C18 cartridge and gradient HPLC. In brief, with a flow rate of 1 ml/min, the mobile phase was changed from 95 % solvent A (0.1 % trifluoroacetic acid (TFA) in water) and 5 % B (0.1 % TFA in acetonitrile (MeCN)) (0–2 min) to 5 % solvent A and 95 % solvent B (2–22 min). UV absorbance was monitored at 254 nm, and the identification of BODIPY 1 dye was confirmed based on the UV spectrum. The purified radiotracer was trapped on C18 cartridge again and eluted with ethanol. An aliquot was taken out and reconstituted in normal saline for *in vitro* and *in vivo* experiments.

Cell Culture and Confocal Imaging of the Cells

Human glioma U87MG cell line and human prostate cancer PC3 cell line were used as surrogates to investigate the molecular mechanisms of ^{18}F BODIPY 1. The U87MG cells were cultured in Minimum Essential Medium Eagle Alpha Modification (α -MEM) supplemented with 10 % fetal bovine serum (FBS) (Sigma). The PC3 cells were cultured in DEME/F12 supplemented with 10 % FBS.

The cells were seeded at 10,000 cells per well on 6-well chamber slides in complete medium and allowed to attached overnight. Then the cells were rinsed briefly with complete medium twice and then incubated with 20 μM ^{18}F BODIPY

1 at 37 °C for 2 h. During the last 20 min, MitoTracker Red (MitoTrackerCMX Ros; Invitrogen, Carlsbad, CA) was added to the wells at a final concentration of 125 nM. After incubation, the cells were washed three times with phosphate-buffered saline (PBS) and fixed in cold methanol for 15 min. The cells were then washed and mounted in Vecta shield mounting medium with 4',6-diamidino-2-phenylindole (DAPI; Vector, Burlingame, CA). The staining was examined using a Zeiss LSM 700 confocal microscope (Carl Zeiss, Thornwood, NY). The images were captured using a $\times 63$ objective and were taken as single image.

Fluorescence Imaging of Primary Brown and White Adipocytes

Primary mouse SVF cells were isolated from interscapular brown fat depots and epididymal white fat depots of C57BL/6 mice and expanded in Dulbecco's modified Eagle's medium (DMEM) supplied with 20 % FBS. Confluent cells were induced for adipogenesis with dexamethasone, 3-isobutyl-1-methylxanthine (IBMX), and insulin until ready for fluorescence staining. DAPI, BODIPY 1, and LipidTOX (Thermo Fisher, H34477) were added to live cell cultures of primary brown and white adipocytes for 1 h. Fluorescence imaging of live cells was done under an EVOS FL fluorescence microscope.

Animal Models

Animal procedures were performed according to a protocol approved by the Institutional Animal Care and Use Committee (IACUC) of the University of North Carolina. A total of 15 female BALB/c mice (9–11 weeks old) and 15 female C57BL/6 mice were purchased from Jackson Laboratory and used in this study. The animals were prepared according to previous report [24]. In brief, the mice were anesthetized with an i.p. injection of 60 mg/kg of pentobarbital (Nembutal, Abbott Laboratories). Core temperature was measured and maintained using a closed loop temperature control system that included a heating lamp and a rectal temperature probe. BAT thermogenesis was stimulated by a subcutaneous injection of norepinephrine (Levophed, Hospira) at a dose of 1 mg/kg. All animals were euthanized at the end of the imaging study for biodistribution study to validate the *in vivo* PET imaging results.

Small Animal PET/CT Imaging Studies

PET/CT scans and image analysis were performed using a small animal PET scanner (GE eXplore Vista) as previously reported [25–27]. [^{18}F]BODIPY 1 (1.85 MBq each) was intravenously injected at 5–10 min after BAT stimulation. Static PET images (10 min) were then acquired at 1 h post injection (p.i.) of [^{18}F]BODIPY 1. The images were

reconstructed by the two-dimensional ordered subset expectation maximum (OSEM) algorithm. For each PET scan, volumes of interest (VOIs) were drawn over the muscle and BAT on decay-corrected whole-body coronal images. The average radioactivity concentration (accumulation) within the organ of interest was obtained from the mean pixel values, which was then converted to counts/ml/min using a conversion factor. Assuming a tissue density of 1 g/ml, the VOIs were converted to counts/g/min and then divided by the administered activity to obtain an image-derived %ID/g.

Biodistribution of [^{18}F]BODIPY 1

Right after PET/CT scans, the mice were euthanized. The blood, heart, and other major organs were collected and wet-weighted. The radioactivity in the tissue was measured using a gamma-counter (PerkinElmer). The results were presented as the percentage injected dose per gram of tissue (%ID/g). Values were expressed as the means \pm SD for each group of animals.

Histological Analysis and Fluorescence Imaging of BAT

Adipose tissue was fixed with 4 % formalin and embedded with paraffin, sliced to 8- μm thickness sections on glass slides, and subjected to H&E staining as described. Meanwhile, BAT tissue was embedded in Tissue-Tec optimal-cutting-temperature compound (Sakura Finetek, Torrance, CA, USA) and cut into 8- μm sections. Frozen sections were covered with EverBrite Mounting Medium containing DAPI and observed directly for the fluorescence of [^{18}F]BODIPY 1 under a Zeiss LSM 700 laser scanning microscope.

Statistical Analysis

Quantitative data were expressed as the means \pm SD. The means were compared using Student's *T* test. *p* values of < 0.05 were considered statistically significant.

Results

Radiochemistry

The F-18 fluorination of BODIPY 1 afforded desired product in 54.9 ± 3.0 % decay-corrected isolation yield with 99 % radio purity. The specific activity (SA) was calculated to be 3.67 ± 0.80 GBq/ μmol (Fig. 1).

Intercellular Localization of [^{18}F]BODIPY 1

After co-incubated with BODIPY 1 and MitoTracker Red, U87MG and PC3 cells were imaged under a confocal microscope. As shown in Fig. 2, BODIPY 1 distributed throughout the cytoplasm after being taken up and co-

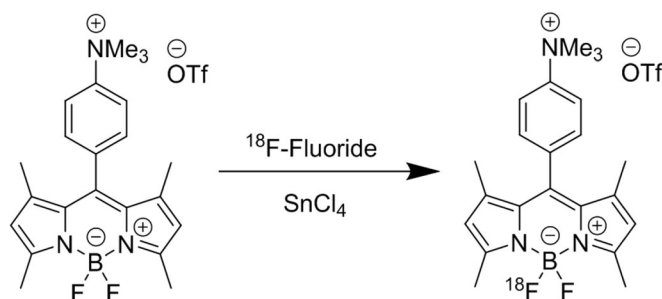


Fig. 1. Preparation of [^{18}F]BODIPY 1.

localized with MitoTracker Red in both cell lines tested. This result is consistent with our previous work [23] and indicates that the uptake of [^{18}F]BODIPY 1 could be the result of its accumulation in the mitochondria. In Fig. 2, we observed variation of fluorescence signal intensities from MitoTracker Red and BODIPY 1 in U87MG cells and PC3 cells. MitoTracker Red probe contains a mildly thiol-reactive chloromethyl moiety; it passively diffuses across the plasma membrane and accumulates in active mitochondria. In U87MG cells, we observed relatively higher MitoTracker Red signal and lower BODIPY 1 signal, while in PC3 cells we observed relatively lower MitoTracker Red signal and higher BODIPY 1 signal. Since the confocal images were acquired using the same parameters, we postulated that BODIPY 1 accumulation in mitochondria may have a different mechanism than MitoTracker Red, and the mitochondria-active status may vary between different cell lines or under different cell conditions.

Fluorescence Imaging of Primary Brown and White Adipocytes

BODIPY 1 targets mitochondria as brown adipocytes contain much more mitochondria than white adipocytes. To validate BODIPY 1 preferably accumulating in brown vs.

white adipocytes, stromal/vascular fractions of interscapular BAT and epididymal WAT were isolated and induced to differentiate into primary brown and white adipocytes *in vitro*, respectively (Fig. 3). Both primary brown and white adipocytes contain many oil droplets as evidenced by LipidTOX fluorescence. Interestingly, primary brown adipocytes have prominent BODIPY 1 fluorescent signal, which does not co-localize with DAPI-stained nuclei or LipidTOX-stained oil droplets. In contrast, primary white adipocytes do not have BODIPY 1 signal. This observation corroborates with our PET imaging and confocal imaging results, suggesting BODIPY 1 could potentially be used to distinguish brown vs. white adipocytes.

Small Animal PET Imaging of BAT

Static PET scans were performed on healthy female BALB/c mice with ($n=8$) or without ($n=6$) norepinephrine stimulation. Selected transverse, coronal, and sagittal PET images of unstimulated and stimulated mice are shown in Fig. 4a. The quantification of major organ activity accumulation in PET scans was realized by measuring the VOIs encompassing the entire organ. The average activity of [^{18}F]BODIPY 1 in the BAT, liver, kidney, and muscle is shown in Fig. 4b. The BAT uptake

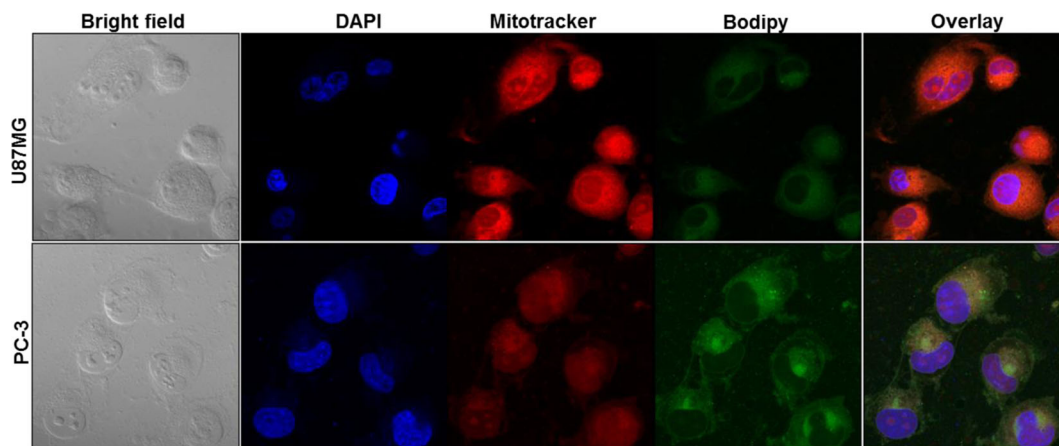


Fig. 2. Confocal imaging of human glioma U87MG cells and human prostate cancer PC3 cells incubated with BODIPY 1 and MitoTracker indicated that BODIPY 1 co-localized with mitochondria upon cellular uptake.

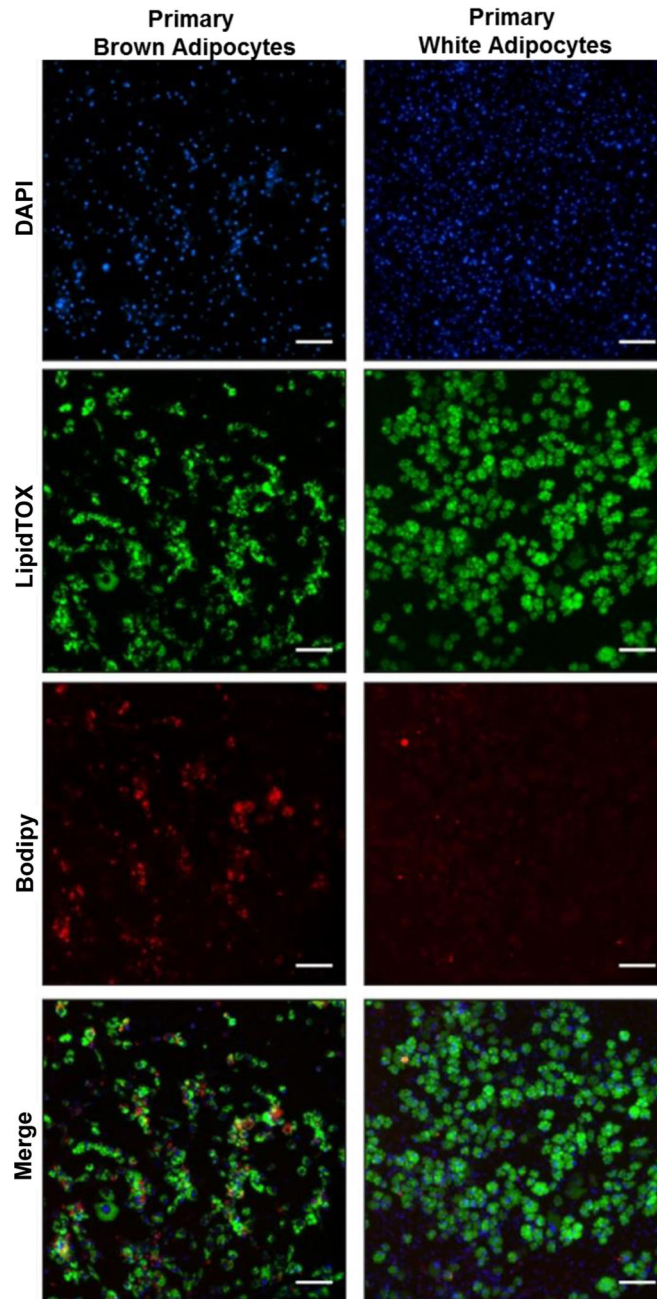


Fig. 3. Fluorescence imaging of primary brown and white adipocytes stained for BODIPY 1, LipidTOX, and DAPI under live cell condition. The primary cells were isolated from interscapular brown fat depots and epididymal white fat depots (purest white fat). The scale bars are 100 μm . The LipidTOX stains for oil droplet. The BODIPY 1 stains in cytoplasm (not overlap with either DAPI or LipidTOX).

of [^{18}F]BODIPY 1 was 3.57 ± 0.54 and 4.78 ± 1.25 %ID/g for unstimulated and stimulated mice at 1 h p.i., respectively. The [^{18}F]BODIPY 1 showed a substantially higher kidney uptake, which was 16.86 ± 2.66 and 13.55 ± 3.27 %ID/g. Student *T* tests indicated that the accumulation of [^{18}F]BODIPY 1 in stimulated BAT was slightly higher than that in non-stimulated BAT (no significant difference, $p > 0.05$). The accumulation of [^{18}F]BODIPY 1 in the liver, kidney, and muscle of the unstimulated and

stimulated BALB/c mice was not significantly different either. In addition, biodistribution of [^{18}F]BODIPY 1 was examined in each mouse at 1.3 h p.i. As shown in Fig. 4c, based on ROI analysis, the BAT uptake of [^{18}F]BODIPY 1 was slightly higher in stimulated (7.763 ± 1.138 %ID/g, $N=10$) mice than that in unstimulated (5.149 ± 0.702 %ID/g, $N=12$) mice, but the difference was not significant according to unpaired two-tailed *T* test ($p = 0.221$).

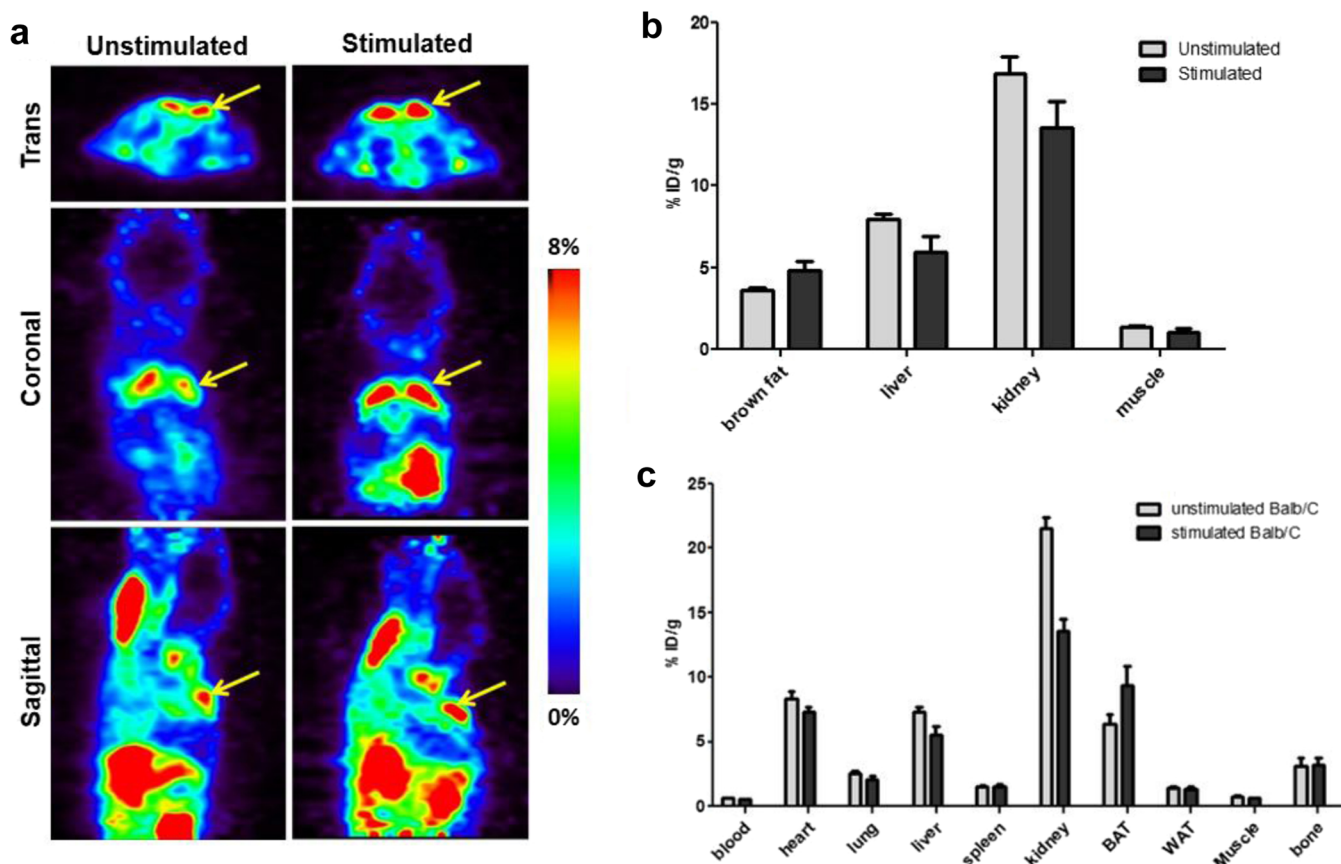


Fig. 4. $[^{18}\text{F}]$ BODIPY 1 PET imaging and biodistribution in BALB/c mice. **a** Representative PET images showing the BAT-specific accumulation of $[^{18}\text{F}]$ BODIPY 1 in unstimulated and stimulated thermogenic mice. **b** Quantitative PET image analysis of $[^{18}\text{F}]$ BODIPY 1 accumulation in major organs including BAT, liver, kidney, and muscle. **c** $[^{18}\text{F}]$ BODIPY 1 distribution in major organs including blood, heart, lung, liver, spleen, kidney, BAT, WAT, and muscle of BALB/c mice. The mice were anesthetized with an i.p. injection of 60 mg/kg of pentobarbital and the radiotracer (1.85 MBq) was applied *via* the lateral tail vein. Static PET images (10 min) were then acquired at 1 h p.i.

Static PET scans were also performed in unstimulated ($n=7$) and stimulated ($n=6$) C57BL/6 mice. Selected transverse, coronal, and sagittal PET images of unstimulated and stimulated mice are shown in Fig. 5a. The average quantification of $[^{18}\text{F}]$ BODIPY 1 in the BAT, liver, kidney, and muscle is shown in Fig. 5b. The BAT uptake of $[^{18}\text{F}]$ BODIPY 1 was 3.48 ± 0.89 and 4.30 ± 1.10 %ID/g for unstimulated and stimulated mice at 1 h p.i., respectively ($p > 0.05$). The distribution of $[^{18}\text{F}]$ BODIPY 1 in C57BL/6 mice was similar to that in BALB/c mice, with kidney having the highest accumulation of 16.58 ± 3.34 and 14.29 ± 2.33 %ID/g for unstimulated and stimulated mice, respectively (Fig. 5b). The biodistribution study of $[^{18}\text{F}]$ BODIPY 1 in C57BL/6 mice was performed in each unstimulated or stimulated C57BL/6 mouse at 1.3 h p.i. As shown in Fig. 5c, the BAT tissue uptake of $[^{18}\text{F}]$ BODIPY 1 was slightly higher in stimulated (6.366 ± 1.090 %ID/g, $n=9$) mice than that in unstimulated (4.273 ± 0.485 %ID/g, $n=9$) mice, but again, the difference was not significant ($p=0.098$). The $[^{18}\text{F}]$ BODIPY 1 uptake was not significantly different between C57BL/6 and BALB/c mice regardless of the BAT

stimulation status (see data above, $p > 0.05$). The PET quantification results and the biodistribution results were consistent in both strains and therefore further validated the *in vivo* distribution pattern of $[^{18}\text{F}]$ BODIPY 1 tracer. Relatively high kidney uptake could be caused by the positive charge and the renal clearance route of the tracer.

Noteworthy, we reported using $[^{18}\text{F}]$ BODIPY 1 as a potential cardiac imaging agent due to its capability to accumulate in the mitochondria [28]. The heart uptake of $[^{18}\text{F}]$ BODIPY 1 was calculated as 4.38 ± 0.46 and 3.51 ± 0.42 %ID/g at 0.5 and 2 h p.i. In this study, we also observed significant heart uptake of $[^{18}\text{F}]$ BODIPY 1, which was not affected by the strain of the mice and the presence or absence of pharmacological stimulation. In BALB/c mice, the heart uptake was 8.35 ± 1.45 and 7.27 ± 0.96 %ID/g in unstimulated and stimulated mice, respectively. While in C57BL/6 mice, the heart uptake was 6.47 ± 1.02 and 5.95 ± 1.21 %ID/g, respectively. To our best knowledge, the direct comparison of BAT PET imaging tracer uptake between different mice strains is scarce. Our study provided preliminary data on the BAT abundance in two popular mice

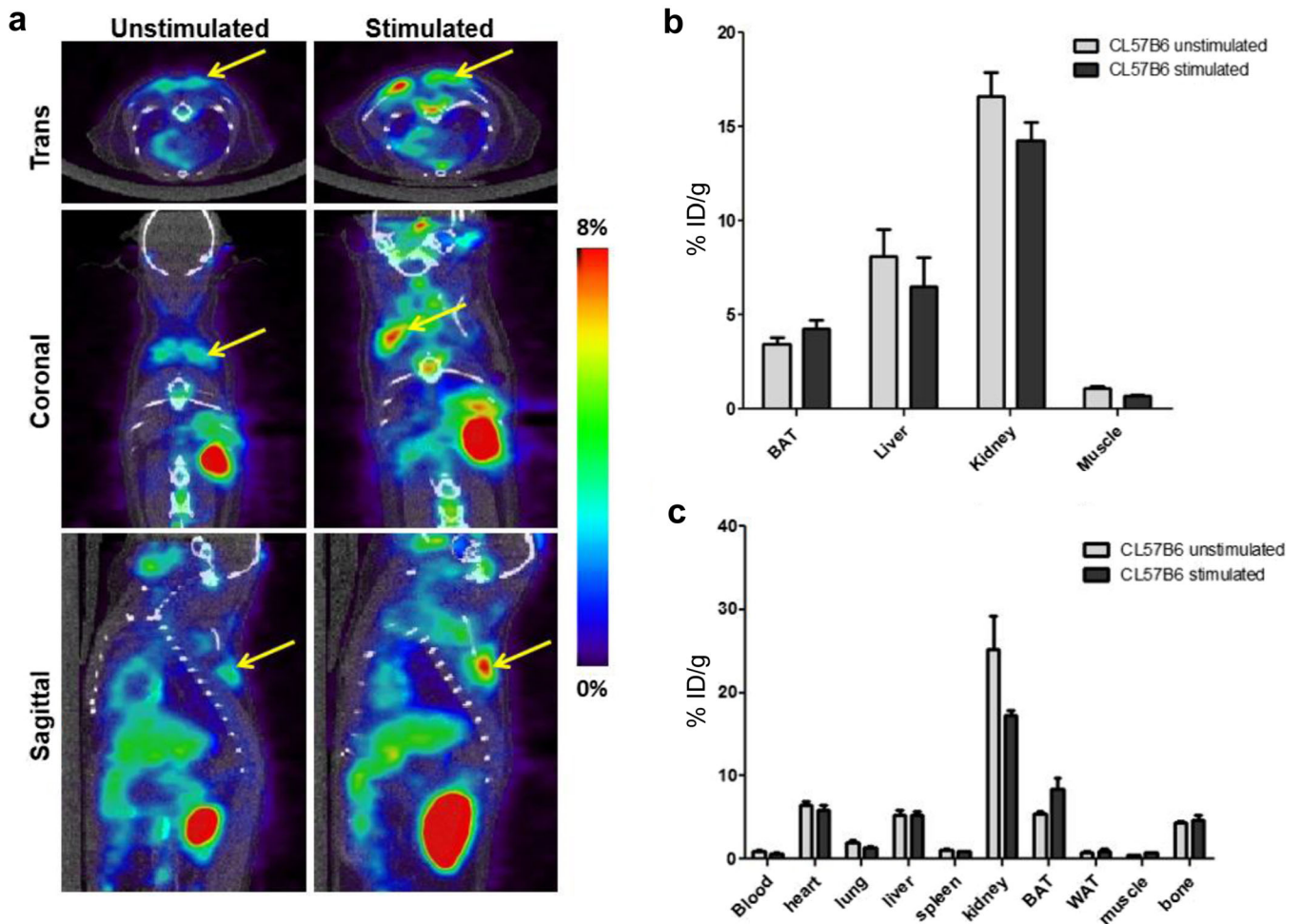


Fig. 5. [^{18}F]BODIPY 1 PET imaging and biodistribution in C57Bl6 mice. **a** Representative PET images showing the BAT-specific accumulation of [^{18}F]BODIPY 1 in unstimulated and stimulated thermogenic mice. **b** Quantitative PET image analysis of [^{18}F]BODIPY 1 accumulation in major organs including BAT, liver, kidney, and muscle of unstimulated and stimulated thermogenic mice. **c** [^{18}F]BODIPY 1 distribution in major organs including blood, heart, lung, liver, spleen, kidney, BAT, WAT, and muscle of unstimulated and stimulated thermogenic C57Bl6 mice. The mice were anesthetized with an i.p. injection of 60 mg/kg of pentobarbital and the radiotracer (1.85 MBq) was applied *via* the lateral tail vein. Static PET images (10 min) were then acquired at 1 h p.i.

strains—BALB/c and C57BL6—which could provide useful information on BAT-related studies using these mice strains.

Histological Examination and Confocal Imaging of the BAT

Histologically, white fat cells are characterized by a single large lipid droplet, flattened and eccentric nuclei, and scanty cytoplasm surrounding the lipid droplet. The morphology of WATs collected from the stimulated and unstimulated mice (Fig. 6a) was not significantly different. In contrast, brown adipocytes have rounded and centrally located nuclei and are polygonal in shape, containing multiple lipid droplets of different sizes that are tucked between numerous mitochondria. While BAT is morphologically very different from

WAT in these mice, the morphology of unstimulated and stimulated BAT was similar.

Since BODIPY 1 itself has fluorescence (excitation = 488 nm; emission = 510–550 nm), we further analyzed the [^{18}F]BODIPY 1 distribution in stimulated and unstimulated BAT. As shown in Fig. 5, while green fluorescence signal could be detected from both unstimulated and stimulated BAT of BALB/C and C57BL6 mice, the signal intensities were higher in stimulated BAT than in unstimulated BAT in both strains. The confocal imaging results were consistent with our *in vivo* PET imaging and biodistribution study results.

Discussion

The detection of BAT remains one of the major challenges for studying BAT. Despite several probes have been

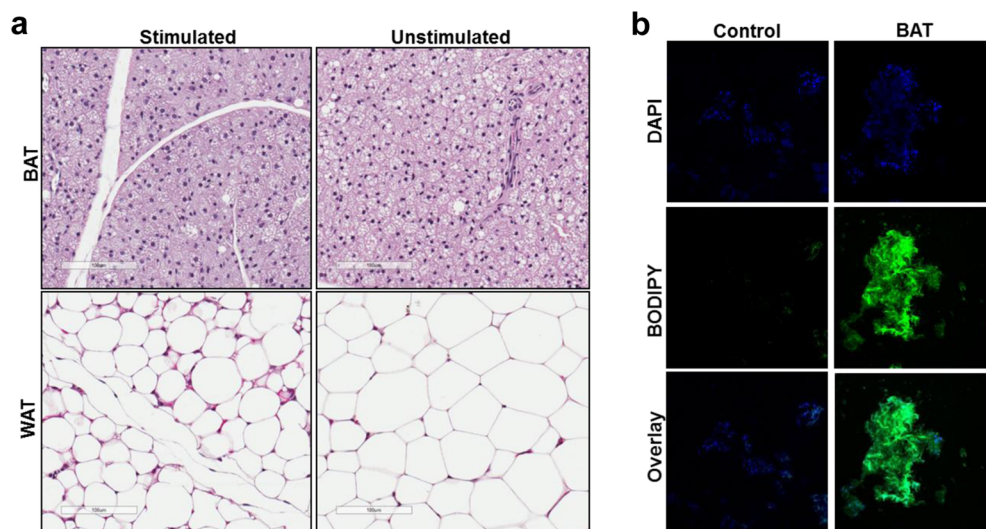


Fig. 6. Histology examination of the BAT and WAT tissues. **a** H&E staining of unstimulated and stimulated WAT and BAT tissues. **b** Confocal imaging of BAT tissue collected from normal mouse without BODIPY 1 injection (control), unstimulated mouse injected with BODIPY 1, and stimulated mouse injection with BODIPY 1. The Ex/Em was 488 nm/520 nm for BODIPY 1 dye. Control BAT showed weak auto fluorescence. In contrast, both unstimulated and stimulated mice received BODIPY 1 injection showed significant strong fluorescence.

designed and used to target and detect BAT, targeting efficiency, especially under basal conditions, remains one of the major roadblocks. Here we investigated the targeting efficiency of a mitochondria-targeting PET probe, [^{18}F]BODIPY 1. [^{18}F]BODIPY 1 easily penetrates cell membranes and is particularly suited to intracellular imaging within living cells. Our result demonstrates that [^{18}F]BODIPY 1 has relatively high uptake in BAT, both under basal conditions and during stimulation of thermogenesis. In the activated state, the uptake of [^{18}F]BODIPY 1 in BAT increased slightly but not significantly, whereas [^{18}F]FDG uptake is considerably increased. In addition, uptake of [^{18}F]BODIPY 1 did not differ between the two mouse phenotypes, the obesity-prone C57BL6 mouse and the obesity-resistant BALB/C mouse used in this study. Taking advantage of its bifunctional properties of BODIPY 1, as fluorescence probe and PET probe, we were also able to assess the intracellular binding of the probe. Cell confocal imaging confirmed that BODIPY 1 co-localized with mitochondria, while *ex vivo* BAT tissue confocal imaging confirmed slightly increased in probe uptake in BAT under stimulation conditions.

Our previous study has shown that the uptake of [^{18}F]BODIPY 1 is dose- and time-dependent [23]. In addition, the decreased cellular uptake in high-potassium conditions confirmed the membrane potential-dependent uptake of [^{18}F]BODIPY 1 could be driven by the plasma and cell membrane potentials. In this study, we further tested the intracellular location of [^{18}F]BODIPY 1. We used tumor cell lines as a surrogate system for this purpose. After co-incubation with [^{18}F]BODIPY 1 and MitoTracker, the cells were observed under a confocal microscope. Our results confirmed that [^{18}F]BODIPY 1 co-localized with

mitochondria. Moreover, taking advantage of BODIPY 1's fluorescent property, [^{18}F]BODIPY 1 can be utilized for synthesizing PET/optical dual modality BAT probes, even in the near-infrared region.

Several mitochondria-targeting probes have been investigated for BAT PET imaging including [^{18}F]fluorobenzyl-triphenylphosphine ([^{18}F]FBnTP) [29–31]. [^{18}F]FBnTP showed a high uptake in BAT under basal condition. However, [^{18}F]FBnTP uptake in BAT decreased by 80 % when the animals were exposed to cold. The decreased uptake of [^{18}F]FBnTP is due to a decrease in mitochondrial membrane voltage when UCP1 is activated. Studies with [$^{99\text{m}}\text{Tc}$]sestamibi also showed high BAT uptake (37.30 ± 14.42 %ID/blood) in unstimulated animals (room temperature) and a slightly increased BAT uptake (1.39-fold; $p = 0.07$) in stimulated animals (exposed to cold for 4 h) [32]. This discrepancy may be partially caused by the mechanism of BAT activation. Cold stimulation increases BAT uptake of [$^{99\text{m}}\text{Tc}$]sestamibi; however, [$^{99\text{m}}\text{Tc}$]sestamibi is known as an agent with high lipophilicity and may wash out when cold activation produces an acute decrease in the fat content of BAT. As a result, the increase [$^{99\text{m}}\text{Tc}$]sestamibi uptake in BAT may have been offset by rapid lipid clearance. In our study, the uptake of [^{18}F]BODIPY 1 showed similar behavior as [$^{99\text{m}}\text{Tc}$]sestamibi. The possible explanation is that both BODIPY 1 and sestamibi accumulate in mitochondria, and the density of mitochondria could be increased by prolonged cold exposure but not by acute cold exposure or short-term pharmacological stimulation.

PET imaging and biodistribution study reveal that [^{18}F]BODIPY 1 has a significant higher uptake in BAT than in WAT. Since under basal condition, blood flow to BAT is not much higher than blood flow to WAT, the

increase uptake of this probe in BAT is unlikely the result of an increase in tissue blood flow. This is also confirmed by our *in vitro* cell studies that show that BODIPY 1 preferentially accumulates in brown adipocytes. The strong uptake of BODIPY 1 is more likely the result of its mitochondria-targeting properties and lipophilic nature. Unlike WAT, BAT is characterized by a high mitochondria density, which is what confers to this tissue its characteristic brown color. The mitochondria density in BAT is among the highest of any tissue. In BAT mitochondria, heat is generated thanks to the presence of UCP1, which, under adrenergic stimulation, uncouples electron transit and ATP production. More importantly, while chronic cold exposure is known to increase mitochondria density in BAT, a recent study showed that acute cold exposure (or activation with norepinephrine) immediately promotes mitochondrial swelling [33]. The NE-induced mitochondrial swelling may be responsible for the slight increase in BODIPY 1 uptake in BAT under stimulatory conditions seen in these studies, or it could simply be the result of the strong increase in blood flow to BAT that is known to occur during adrenergic stimulation. Either way, the results of this study raise an intriguing possibility to visualize BAT thermogenic capacity, which is strongly coupled with tissue mitochondria density, using [¹⁸F]BODIPY 1 PET scan in adult humans. More importantly, the ability of this probe to equally target stimulated and unstimulated BAT represents a major advantage over current probes like [¹⁸F]FDG that require acute cold or adrenergic stimulation for detection[34]. Such imaging approach has unique advantages in that [¹⁸F]FDG PET imaging of BAT, the current “gold standard” of BAT visualization, relies on the activation of BAT after cold or drug stimulation. In contrast, [¹⁸F]BODIPY 1 probe in the present study shows preferable accumulation in BAT (comparing to WAT) under unstimulated conditions, which has great clinical implications for patients with associated risks from cold stress or sympathetic activation.

PET imaging allows *in vivo* non-invasive assessment of areas with changed functionality (*e.g.*, blood flow, metabolism, receptor density). One particular strength of the PET technique is its high sensitivity. However, due to the intrinsic physics limits of PET and the scanner design, relatively poor (4–6 mm) spatial resolution (SR) is the weakest point of PET technique. Because of the finite SR, the radioactivity coming from neighboring regions is mixed and blurred, which reduces the image contrast, limits the detectability of small lesions, and prevents precise anatomical localization of focal radiotracer uptake. The phenomenon is called partial volume effect (PVE). PVE affects PET image both qualitatively and quantitatively. The PVE becomes particularly significant when the target region is smaller than 2–3 times the system’s full width at half maximum (FWHM), as it is in brain structures, small tumors, and in this study, mouse BAT. Partial volume correction (PVC) strategies include methods that based on recovery coefficients, and techniques using high-resolution

structural information extracted from co-registered CT or MR images [35]. In this study, we drew ROIs over BAT delineated on co-registered CT images in an attempt to compensate PVE. However, due to intrinsic weakness of CT images, the BAT had poor contrast with surrounding tissue. To further validate the quantitative PET analysis results, we performed biodistribution study and calculated accurate [¹⁸F]BODIPY 1 in BAT based on gamma counting and tissue weight.

Conclusions

The study demonstrated that [¹⁸F]BODIPY 1 accumulates predominantly in BAT. Co-localization of BODIPY 1 and MitoTracker indicates that this probe, upon cellular uptake, targets cell mitochondria. Because [¹⁸F]BODIPY 1 can preferably accumulate in mitochondria-rich BAT, regardless of its activation state and animal strains, we propose here that [¹⁸F]BODIPY 1 could potentially be used to quantitate BAT abundance and therefore could facilitate the non-shivering thermogenesis and oxidative metabolism-related studies.

Funding Information. This study was supported by Start-Up grant from the Department of Radiology, University of North Carolina at Chapel Hill (Z.W.) and R01DK108231 (R.T.B.).

Compliance with Ethical Standards.

Animal procedures were performed according to a protocol approved by the Institutional Animal Care and Use Committee (IACUC) of the University of North Carolina.

Conflict of Interest

The authors declare that they have no conflict of interest.

References

1. Gesta S, Tseng YH, Kahn CR (2007) Developmental origin of fat: tracking obesity to its source. *Cell* 131:242–256
2. Himms-Hagen J (2001) Does brown adipose tissue (BAT) have a role in the physiology or treatment of human obesity? *Rev Endocr Metab Disord* 2:395–401
3. Nedergaard J, Bengtsson T, Cannon B (2007) Unexpected evidence for active brown adipose tissue in adult humans. *Am J Physiol Endocrinol Metab* 293:E444–E452
4. Bartelt A, Heeren J (2012) The holy grail of metabolic disease: brown adipose tissue. *Curr Opin Lipidol* 23:190–195
5. Guerra C, Navarro P, Valverde AM, Arribas M, Brüning J, Kozak LP, Kahn CR, Benito M (2001) Brown adipose tissue-specific insulin receptor knockout shows diabetic phenotype without insulin resistance. *J Clin Invest* 108:1205–1213
6. Lee P, Zhao JT, Swarbrick MM, Gracie G, Bova R, Greenfield JR, Freund J, Ho KKY (2011) High prevalence of brown adipose tissue in adult humans. *J Clin Endocrinol Metab* 96:2450–2455
7. Cannon B, Nedergaard J (2004) Brown adipose tissue: function and physiological significance. *Physiol Rev* 84:277–359
8. Muzik O, Mangner TJ, Leonard WR, Kumar A, Janisse J, Granneman JG (2013) ¹⁵O PET measurement of blood flow and oxygen consumption in cold-activated human brown fat. *J Nucl Med* 54:523–531

9. Rothwell NJ, Stock MJ (1979) A role for brown adipose tissue in diet-induced thermogenesis. *Nature* 281:31–35
10. Lee P, Greenfield JR, Ho KK, Fulham MJ (2010) A critical appraisal of the prevalence and metabolic significance of brown adipose tissue in adult humans. *Am J Physiol Endocrinol Metab* 299:E601–E606
11. Jacene HA, Cohade CC, Zhang Z, Wahl RL (2011) The relationship between patients' serum glucose levels and metabolically active brown adipose tissue detected by PET/CT. *Mol Imaging Biol* 13:1278–1283
12. Chang L, Milton H, Eitzman DT, Chen YE (2013) Paradoxical roles of perivascular adipose tissue in atherosclerosis and hypertension. *Circ J* 77:11–18
13. Kortelainen ML (1996) Association between cardiac pathology and fat tissue distribution in an autopsy series of men without premortem evidence of cardiovascular disease. *Int J Obes Relat Metab Disord* 20:245–252
14. Inokuma K, Ogura-Okamatsu Y, Toda C, Kimura K, Yamashita H, Saito M (2005) Uncoupling protein 1 is necessary for norepinephrine-induced glucose utilization in brown adipose tissue. *Diabetes* 54:1385–1391
15. Hanssen MJ, van der Lans AA, Brans B et al (2015) Short-term cold acclimation recruits brown adipose tissue in obese humans. *Diabetes* 65:1179–1189
16. Rossato M, Cecchin D, Vettor R (2016) Brown adipose tissue localization using ^{18}F -FDG PET/MRI in adult. *Endocrine* 54:562–563
17. Lahesmaa M, Orava J, Schalin-Jantti C et al (2014) Hyperthyroidism increases brown fat metabolism in humans. *J Clin Endocrinol Metab* 99:E28–E35
18. Min JJ, Biswal S, Deroose C, Gambhir SS (2004) Tetraphenylphosphonium as a novel molecular probe for imaging tumors. *J Nucl Med* 45:636–643
19. Admiraal WM, Holleman F, Bahler L, Soeters MR, Hoekstra JB, Verberne HJ (2013) Combining 123I-metaiodobenzylguanidine SPECT/CT and ^{18}F -FDG PET/CT for the assessment of brown adipose tissue activity in humans during cold exposure. *J Nucl Med* 54:208–212
20. Hadi M, Chen CC, Whatley M, Pacak K, Carrasquillo JA (2007) Brown fat imaging with ^{18}F -6-fluorodopamine PET/CT, ^{18}F -FDG PET/CT, and ^{123}I -MIBG SPECT: a study of patients being evaluated for pheochromocytoma. *J Nucl Med* 48:1077–1083
21. Izzi-Engbeaya C, Salem V, Atkar RS, Dhillo WS (2015) Insights into brown adipose tissue physiology as revealed by imaging studies. *Adipocyte* 4:1–12
22. Cypess AM, Doyle AN, Sass CA, Huang TL, Mowschenson PM, Rosen HN, Tseng YH, Palmer EL, Kolodny GM (2013) Quantification of human and rodent brown adipose tissue function using $^{99\text{m}}\text{Tc}$ -methoxyisobutylisonitrile SPECT/CT and ^{18}F -FDG PET/CT. *J Nucl Med* 54:1896–1901
23. Liu S, Li D, Shan H, Gabbai FP, Li Z, Conti PS (2014) Evaluation of ^{18}F -labeled BODIPY dye as potential PET agents for myocardial perfusion imaging. *Nucl Med Biol* 41:120–126
24. Branca RT, He T, Zhang L, Floyd CS, Freeman M, White C, Burant A (2014) Detection of brown adipose tissue and thermogenic activity in mice by hyperpolarized xenon MRI. *Proc Natl Acad Sci U S A* 111:18001–18006
25. Chansaenpak K, Wang M, Wu Z, Zaman R, Li Z, Gabbai FP (2015) [^{18}F]-NHC-BF₃ adducts as water stable radio-prosthetic groups for PET imaging. *Chem Commun (Camb)* 51:12439–12442
26. Deng H, Wang H, Wang M, Li Z, Wu Z (2015) Synthesis and evaluation of ^{64}Cu -DOTA-NT-Cy5.5 as a dual-modality PET/fluorescence probe to image neurotensin receptor-positive tumor. *Mol Pharm* 12:3054–3061
27. Selvaraj R, Giglio B, Liu S, Wang H, Wang M, Yuan H, Chintala SR, Yap LP, Conti PS, Fox JM, Li Z (2015) Improved metabolic stability for ^{18}F PET probes rapidly constructed via tetrazine trans-cyclooctene ligation. *Bioconjug Chem* 26:435–442
28. Chansaenpak K, Wang H, Wang M, Giglio B, Ma X, Yuan H, Hu S, Wu Z, Li Z (2016) Synthesis and evaluation of [^{18}F]-ammonium BODIPY dyes as potential positron emission tomography agents for myocardial perfusion imaging. *Chemistry* 22:12122–12129
29. Madar I, Isoda T, Finley P, Angle J, Wahl R (2011) ^{18}F -fluorobenzyl triphenyl phosphonium: a noninvasive sensor of brown adipose tissue thermogenesis. *J Nucl Med* 52:808–814
30. Madar I, Ravert H, Nelkin B, Abro M, Pomper M, Dannals R, Frost JJ (2007) Characterization of membrane potential-dependent uptake of the novel PET tracer ^{18}F -fluorobenzyl triphenylphosphonium cation. *Eur J Nucl Med Mol Imaging* 34:2057–2065
31. Madar I, Ravert H, Dipaula A et al (2007) Assessment of severity of coronary artery stenosis in a canine model using the PET agent ^{18}F -fluorobenzyl triphenyl phosphonium: comparison with $^{99\text{m}}\text{Tc}$ -tetrofosmin. *J Nucl Med* 48:1021–1030
32. Baba S, Engles JM, Huso DL, Ishimori T, Wahl RL (2007) Comparison of uptake of multiple clinical radiotracers into brown adipose tissue under cold-stimulated and nonstimulated conditions. *J Nucl Med* 48:1715–1723
33. Wikstrom JD, Mahdavi K, Liesa M et al (2014) Hormone-induced mitochondrial fission is utilized by brown adipocytes as an amplification pathway for energy expenditure. *EMBO J* 33:418–436
34. Chalfant JS, Smith ML, Hu HH, Dorey FJ, Goodarzi F, Fu CH, Gilsanz V (2012) Inverse association between brown adipose tissue activation and white adipose tissue accumulation in successfully treated pediatric malignancy. *Am J Clin Nutr* 95:1144–1149
35. Alavi A, Werner TJ, Høiland-Carlsen PF, Zaidi H (2018) Correction for partial volume effect is a must, not a luxury, to fully exploit the potential of quantitative PET imaging in clinical oncology. *Mol Imaging Biol* 20:1–3